Optics Letters

Coherent MIMO radar network enabled by photonics with unprecedented resolution

Salvatore Maresca,[1] Filippo Scotti,[2] Giovanni Serafino,[1] Leonardo Lembo,[1,3] Antonio Malacarne,[1] Fabio Falconi,[2] Paolo Ghelfi,[2] and Antonella Bogoni[1,2,*]

[1]TeCIP Institute, Scuola Superiore Sant'Anna, Via Moruzzi 1, 56124 Pisa, Italy
[2]National Laboratory of Photonic Networks, Inter-University National Consortium for Telecommunications (CNIT), Via Moruzzi 1, 56124 Pisa, Italy
[3]Italian Navy, Naval Research Center CSSN, Vallauri Institute, Italy
*Corresponding author: antonella.bogoni@cnit.it

Received 5 March 2020; revised 13 May 2020; accepted 15 May 2020; posted 19 May 2020 (Doc. ID 391296); published 10 July 2020

The conventional concept of radar is based on stand-alone and independent apparatuses. Superior performance is possible, exploiting distributed points of view (i.e., distributed radars) and centralized data fusion, but systems based only on radio-frequency technology are not able to guarantee the requested degree of coherence and high capacity links among radars. In the current distributed systems, radars act almost independently from each other. Thus, data fusion, which must be performed on locally pre-processed information, can only exploit partial information content, harming the imaging capability of the distributed system. Here we present, to the best of our knowledge, the first extended analysis and experiment of a distributed coherent multiple input-multiple output radar system, enabled by photonics, which maximizes the information content extracted by a centralized data fusion, providing unprecedented resolution capabilities. Stepping from previous achievements, where photonics has been demonstrated in single radars, here photonics is used also for providing coherence and high capacity links among radars. The numerical analysis also demonstrated the benefits of coherent multi-band operation for sidelobe reduction, i.e., false alarms reduction.

https://doi.org/10.1364/OL.391296

Most of the applications of remote microwave sensing like automotive, traffic surveillance, borders control, medical imaging, and environmental monitoring, present ever-increasing operational needs that can be met by distributed multistatic radars [1–4], which represent a breakthrough overcoming the traditional concept of stand-alone radar systems. A specific subset of distributed radars is represented by multiple input-multiple output (MIMO) radar systems, characterized by a deeper degree of cooperation among the radar nodes. These systems can observe the same scene from different viewpoints, employing multiple coherent transmit waveforms, and can jointly process, in a centralized manner, signals acquired by widely separated nodes [3,5–9].

Compared to stand-alone radars, these features grant increased flexibility and power efficiency [10,11], as well as improved target detection and localization capabilities [8,12]. Thanks to the information enhancement granted by MIMO spatial diversity [3], benefits are noticeable especially when attempting to detect low-observable targets, e.g., characterized by high angular variability of the radar cross-section [13], or targets obscured by clutter or other nearby targets. Moreover, MIMO radars permit to increase the cross-range (i.e., angular) resolution [14]. In fact, if single radar range resolution is simply determined by the bandwidth of the transmitted signal, the cross-range resolution depends on the antenna beam aperture and the target distance; MIMO radars, by behaving like sparse antenna arrays, achieve an excellent cross-range resolution independent of antenna features [3], with the additional capability of measuring different components of the target velocity vector from the Doppler frequency shift [15]. Moreover, MIMO radars offer high flexibility in terms of waveform selection and beam pattern synthesis [16]. Thanks to the increased detection, localization, and parameter estimation capabilities [8,9,12,15,17], as well as their versatility, MIMO radars hold the potential to be a key tool in future monitoring systems.

Today, distributed radars do exist [1–3], but with decentralized data fusion: each radar node independently performs its own local processing on the received signals, sending information to the central node for fusion, inevitably losing information [18]. Conversely, MIMO radars can theoretically extract the whole information content [3,17,19], since all the raw received signals are jointly processed. Unfortunately, coherent MIMO radar systems do not exist yet. Their real implementation, especially with widely separated antennas, is still limited and hindered by two main issues: (1) the need for extremely precise time synchronization and, consequently, high phase coherence between all the nodes of the distributed system; and (2) the need for high capacity data links to route the raw data from/to the remote nodes to/from the central node. Phase mismatches may lead to a significant degradation in target detection [20], and the application of additional algorithms for correcting these mismatches leads to an exploding increase of the complexity and computational load of the overall processing chain. Finding viable electronics-based solutions to these problems is very challenging [21]. However, the pioneering photonics-based radar

transceiver [22,23] has opened the way to new research perspectives, stimulating the interest also in MIMO radar applications [24,25].

Recently, photonics has been proposed and successfully demonstrated in a number of key radar functionalities: (1) joint frequency up- and down-conversion with remarkable frequency flexibility and phase stability [22], (2) software-defined coherent multi-band operation [23,26], and (3) coherent radio-frequency (RF) signal routing over optical fiber links [21,27].

This Letter reports on the development and test of an innovative coherent distributed multi-band MIMO radar. In this novel architecture, shown in Fig. 1(A), N RF signals, whose carrier frequencies are denoted with $RF_1 ... RF_N$, are coherently generated/received by means of a single optical local oscillator, placed in the photonic core of a central unit, and delivered/collected to/from M widely distributed radar heads (RHs), by exploiting photonics-based RF signal routing via optical fiber. This ensures a frequency flexibility and a phase stability unknown in standard electronics-based radars [21–24]. As detailed in Fig. 1(B), the photonics-based up- and down-conversions rely on a distributed architecture with a stage in the central unit, shared among all the RHs, and a further dedicated stage in each RH, guaranteeing signal coherence among all the transmitted and received signals.

From the point of view of cross-range resolution enhancement, coherence is fundamental [3]. In MIMO radars, the sparse configuration of the antenna elements (i.e., the distributed RHs) results in the presence of sidelobes in the 2D detection map, that could seriously affect system performance, giving rise to false target detections and localization errors [28].

However, it is demonstrated here that sidelobes can be reduced either by optimizing the system geometry, e.g., acting on the number of RHs, or by opting for multi-band operation, without changing the system geometry nor the RHs number. Thanks to the intrinsic signal coherence granted by photonics, with no need of further synchronization algorithms [29], the signal processing effort required for merging multi-sensor, multi-band signal acquisitions just linearly increases with the number of signal channels.

With reference to Fig. 2, the novel coherent multi-band MIMO radar system has been implemented and outdoor tested in a 2 × 2 configuration, i.e., with two transmitters (TXs) and two receivers (RXs). The antennas, whose positions along a

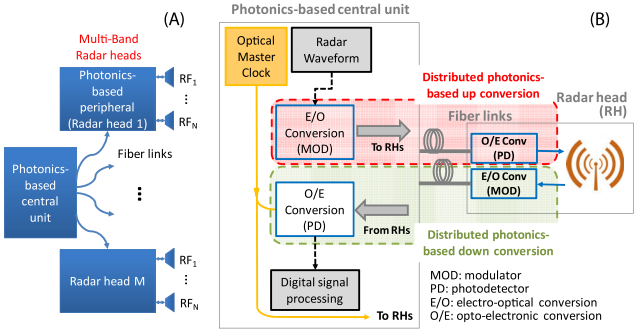

Fig. 1. (A) Working principle of a photonics-based coherent MIMO radar network; (B) structure of a photonics-based coherent MIMO radar network, where the distributed photonics-based up- and down-conversion are highlighted in red and green, respectively.

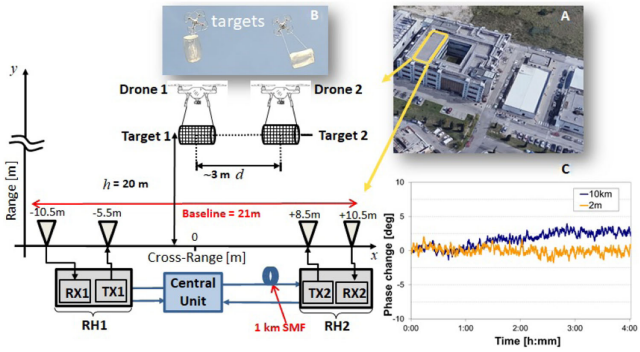

Fig. 2. Architecture of the coherent photonics-based 2 × 2 MIMO radar experiment with the aerial view of the experiment area (inset A), the picture of the used targets (inset B), i.e., two cylinders in metal net suspended to small quad-copter drones and the phase stability of the received signal (inset C). ODL, optical delay line.

21 m-long linear baseline have been optimized through simulations, enable a 2D imaging of the monitored area in both the range and cross range. The best antenna configuration has been chosen based on the maximization of the peak-max sidelobe ratio (PMSR) and the peak-average sidelobe ratio (PASR) metrics [30]. The derivation of generalized criteria for optimizing the MIMO antenna configuration is a complex task, needing a more extensive analysis. A detailed investigation of this matter is currently underway.

The system consists of a central unit with a photonic core, and two RHs with one TX and one RX each. As reported in Fig. 3, the master clock inside the photonic core is constituted by a solid-state mode-locked laser (MLL). This pulsed laser, with a repetition frequency $f_{MLL} = 400$ MHz, allows generating RF carriers with extremely low phase noise [31]. On the TX side, the radar signal, digitally generated at intermediate frequency (IF) by an arbitrary waveform generator (AWG), modulates the MLL spectrum by means of a 20-GHz Mach-Zehnder electro-optic modulator (MOD). Then it is optically routed to the RHs, and there, photodetected by a 20-GHz photodiode (PD). Both the MOD, implemented as a Mach–Zehnder modulator (MZM), and the PD, have bandwidths equal to 20 GHz. This operation generates many signal replicas, each centered at $k \cdot f_{MLL} \pm f_{IF}$, with k positive integer [21,22]. The desired RF output carrier frequency f_{RF} can be selected by means of a pass-filter, centered at f_{RF} and with a bandwidth greater or equal to the signal bandwidth B. This way, the photonics-based up-conversion is carried out. For the employed multi-cavity filters, $B = 100$ MHz and $f_{RF} = 9.7$ GHz. At the TXs, the employed antennas are ultra-wideband Vivaldi-shaped horn antennas with about 50° half-power beam width and 12 dBi maximum gain. The detected radar echoes, received by the RXs with similar antennas, are amplified and pass-band filtered. Then, the RF signal is electrical to optical (E/O) converted by modulating the MLL (sent to the RHs by dedicated links), then transmitted back to the photonic core and optical to electrical (O/E) converted at the PD. This generates replicas of the RF signal at $k \cdot f_{MLL} \pm f_{IF}$, including the replica at IF (for $k = 0$) $f_{IF} = 100$ MHz [21], thus performing down-conversion. Then, the signals from each RX are low-pass filtered and fed into a two-channel analog-to-digital converter (ADC) at 400 MS/s/ch.

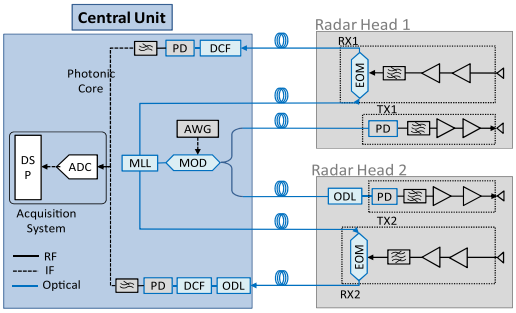

Fig. 3. Setup of the implemented coherent photonics-based 2 × 2 MIMO radar. DSP, digital signal processing; EOM, electro-optical modulator.

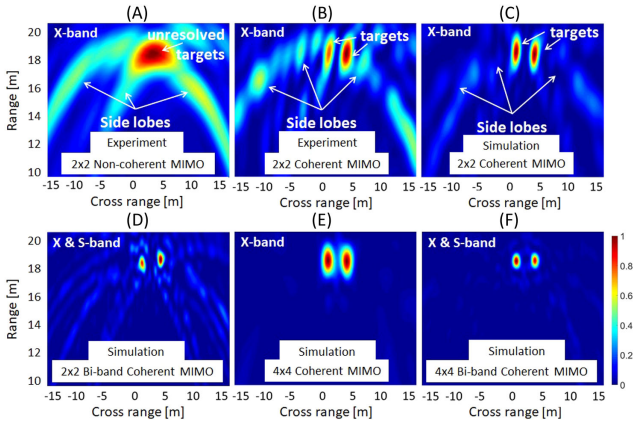

Fig. 4. Range/cross-range map using a 2 × 2 configuration and two targets in the experimental case with an X-band signal and (A) non-coherent or (B) coherent MIMO processing, in the simulative case (C) with coherent MIMO processing and X-band signal and (D) with bi-band signals (X and S bands), (E) using a 4 × 4 configuration in the simulative case with X-band signal and (F) bi-band signals.

Linear frequency-modulated (LFM) pulses with 100 ns duration and 100 MHz bandwidth have been used, with a transmitted power of 100 mW per antenna. TX1 and TX2 transmitted an up- and down-chirp, respectively. Furthermore, the signals have been separated also in the time domain through a 1 km-long single-mode fiber (SMF) span acting as an optical delay line inserted between the central unit and RH2 (Fig. 2), with a delay of 5 μs between the two transmitted signals, to ensure an appropriate signal orthogonality. A 50 μs pulse repetition interval has been used, corresponding to a non-ambiguous range of ~ 7.5 km.

A span of dispersion compensating fiber (DCF) in the central unit broadens the received pulses, reducing the peak power at the PD input. The photonic core and the RHs are connected through spans of SMF. All optical links do not heavily affect the signal synchronization. Fluctuations due to mechanical stress can be neglected, while a proper calibration procedure can compensate for a slow phenomenon like temperature fluctuations. In Fig. 2 (inset C), the phase stability of the received signal at the central unit over a period of 4 h, measured using a 10 km (blue line) and a 2 m (yellow line) fiber spool, is reported, to evaluate the optical link impact. The measurement confirms that long fiber spools have a negligible effect on the short period, but they introduce a slight drift of about 5° over multiple hours, due to thermal fluctuations. If not compensated for with a proper calibration procedure over many hours, this could in principle affect the performance of the MIMO processing. However, as long as the angular jitter of the architecture is lower than 10^{-1} rad (i.e., 6°), the effects on the MIMO coherent detection performance are negligible [32].

The targets used in the experiment were two cylinders made of metal net suspended to small quad-copter drones, kept approximately 3 m spaced from each other, at a range distance of ≈ 15−20 m from the radar baseline. After a pre-processing stage, the experimental data have undergone both non-coherent and coherent MIMO radar processing [3,33]. The first output is calculated from the non-coherent super-position of the single bistatic detection maps (i.e., the cross-correlation matrices after 2D mapping in the range/cross-range space). The second output stems from the same detection maps, which can be summed together coherently [3]. A comparison between non-coherent and coherent MIMO radar processing shows the benefits introduced by the coherence. Simulations have been run to confirm the experimental results and to investigate more complex scenarios, as well as the impact of the sensor number and of the multi-band operation on the system performance. These simulations have been performed replicating the experimental conditions of the field trial, with some necessary simplification assumptions: (1) the two targets have been considered as single point-like scatterers at the same positions measured by the radar, which have been assumed to be the ground-truth data for the simulations; (2) no background clutter has been considered in the simulations. In fact, the transmitted power was low, and the network was deployed, according to the scheme in Fig. 2, with the four antennas oriented upwards, to mitigate any possible clutter and multipath return from the surrounding structures. Finally, a cell averaging constant false alarm rate (CA-CFAR) algorithm has been used to estimate the system detection capability [34].

Figures 4(A) and 4(B) report the results in a single-band configuration, showing the experimental range/cross-range maps obtained performing non-coherent and coherent MIMO processing on the received data. It is well evident that the cross-range resolution improves, thanks to the coherence, thus allowing us to clearly distinguish the two targets at about 3 m from each other. The antenna aperture at the target distance (∼18 m) gives a cross-range resolution of >15 m (without MIMO processing). The non-coherent MIMO processing allows us to reduce to 10 m (i.e., not enough to distinguish the two targets), while the coherent MIMO processing introduces a further significant improvement, down to about 2.4 m, corresponding to a > 5-fold enhancement compared to the monostatic radar case. Yet, sidelobes are not negligible, and they may lead to false detections.

The simulated result, shown in Fig. 4(C) and obtained considering the same parameters as in the experiment, is close to the real output of Fig. 4(B). Stepping from these similarities, the tool has been used for simulating also different MIMO radar system configurations. The coherent MIMO output of the same 2 × 2 system operated in dual-band configuration is depicted in Fig. 4(D). Here the coherent fusion of the signals in the S and X bands (i.e., with $f_{RF}(S) = 2.6$ GHz and $f_{RF}(X) = 9.7$ GHz) brings an overall reduction of the maximum amplitude of sidelobes, as well as an improvement of the range and cross-range resolutions by a factor ≈2.6 (i.e., from 1.85 to 0.72 m) and

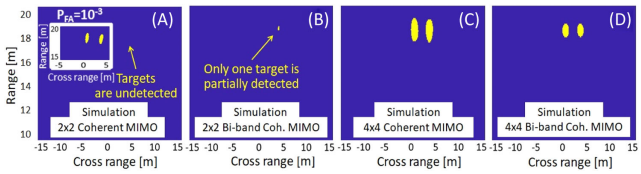

Fig. 5. Detection maps of the simulated cases reported in Figs. 4(C)–4(F), coherent MIMO processing using a CA-CFAR algorithm with false alarm probability $P_{FA} = 10^{-6}$ (A) with a 2×2 single-band configuration; (B) 2×2 bi-band configuration; (C) 4×4 single-band configuration; and (D) 4×4 bi-band configuration. Since the targets in (A) are not visible, the added inset is for $P_{FA} = 10^{-3}$, where the targets can be correctly detected.

$\approx$ 1.6 (i.e., from 1.26 to 0.78 m), respectively. Instead, if the single-band MIMO sensor configuration is increased from 2×2 [as in Fig. 4(C)] to 4×4 [Fig. 4(E)], we observe a significant reduction of the sidelobes, while the range and cross-range resolutions appear almost unaffected, on average. Finally, when the simulated system exploits both the dual-band and 4×4 distributed MIMO radar configuration, the measured range and cross-range resolutions are 0.74 and 1.0 m, respectively. As shown in Fig. 4(F), we also observe a significant sidelobe mitigation with respect to the 2×2 dual-band system of Fig. 4(D), while resolution metrics are substantially unchanged. The precision in estimating the target position improves, increasing the number of antennas. In fact, the precision, defined as the root mean square error between the target positions measured experimentally and those estimated by simulation, varies between 9.2 cm in Fig. 4(D) and 4.0 cm in Figs. 4(C) and 4(F) for the leftmost target, and from 12.4 cm in Fig. 4(D) to 3.6 cm in Fig. 4(F) for the rightmost target. This result agrees with the concept of diversity gain, i.e., more distributed viewpoints allow a better target detection and localization of the target [3].

Figure 5 reports the detection maps of the simulated cases presented in Figs. 4(C)–4(F), applying the CA-CFAR detection algorithm and setting a detection threshold to obtain a false alarm probability $P_{FA} = 10^{-6}$, which represents the typical requested value in most of the real systems [13]. It is evident that, in the single-band 2×2 scenario, the obtained results are not enough to guarantee the requested detection capabilities and the targets are not correctly detected [Fig. 5(A): in fact, with the set threshold the targets are missed]. A correct detection can be achieved only setting a higher target false alarm probability up to $P_{FA} = 10^{-3}$ [inset in Fig. 5(A)]. On the other hand, the use of either a dual-band operation [Fig. 5(B)] or an increased number of sensors [Fig. 5(C)], or both approaches [Fig. 5(D)], allows us to detect the targets with $P_{FA} = 10^{-6}$.

Funding. North Atlantic Treaty Organization SOLE Project (G5267).

Disclosures. The authors declare no conflicts of interest.

REFERENCES

1. V. S. Chernyak, *Fundamentals of Multisite Radar Systems* (Gordon and Breach, 1998).
2. T. Derham, S. Doughty, K. Woodbridge, and C. J. Baker, *CIE International Conference on Radar* (2006).
3. A. M. Haimovich, R. S. Blum, and L. J. Cimini, IEEE Sig. Proc. Mag. **25**(1), 116 (2008).
4. C. J. Baker and A. L. Hume, Aerosp. Electr. Sys. Mag. **18**(2), 3 (2003).
5. D. W. Bliss and K. W. Forsythe, *Proc. of the 37th Asilomar Conf. on Signals, Systems, and Computers*, California, USA (2003), p. 54.
6. D. Rabideau and P. Parker, *Proc. of the 37th Asilomar Conf. on Signals, Systems, and Computers*, California, USA (2003), p. 1057.
7. F. C. Robey, S. Coutts, D. Weikle, J. C. McHarg, and K. Cuomo, *Proc. of the 37th Asilomar Conf. on Signals, Systems, and Computers*, California, USA (2004), p. 300.
8. I. Bekkerman and J. Tabrikian, IEEE Trans. Signal Process. **54**, 3873 (2006).
9. E. Fishler, A. Haimovich, R. S. Blum, L. J. Cimini, D. Chizhik, and R. A. Valenzuela, IEEE Trans. Signal Process. **54**, 823 (2006).
10. H. Godrich, A. M. Haimovich, and R. S. Blum, IEEE Trans. Inf. Theory **56**, 2783 (2010).
11. S. Fletcher and F. C. Robey, *Presented at 11th Conf. on Adaptive Sensors Array Processing* (2003).
12. L. Xu, J. Li, and P. Stoica, *IEEE Workshop Sensor Array and Multi-Channel Processing*, Massachusetts, USA, July, 2006, p. 258.
13. M. Skolnik, *Introduction to Radar Systems* (McGraw-Hill, 2001).
14. N. H. Lehmann, A. M. Haimovich, R. S. Blum, and L. Cimini, *Proc. of the 40th Asilomar Conf. on Signals, Systems, and Computers*, Massachusetts, USA, November, 2006, p. 25.
15. N. H. Lehmann, A. M. Haimovich, R. S. Blum, and L. Cimini, *Proc. of the 40th Asilomar Conf. on Signals, Systems, and Computers*, Massachusetts, USA, July, 2006.
16. D. R. Fuhrmann and G. Antonio, *Proc. of the Thirty-Eighth Asilomar Conference on Signals, Systems and Computers*, California, USA, November, 2004, p. 295.
17. D. Maio and M. Lops, IEEE Trans. Aerosp. Electron. Syst. **43**, 886 (2007).
18. D. L. Hall and J. Llinas, Proc. IEEE **85**, 6 (1997).
19. A. Gorji, R. Tharmarasa, and T. Kirubarajan, IEEE Trans. Aerosp. Electron. Syst. **49**, 2179 (2013).
20. M. Akcakaya and A. Nehorai, *Proc. of the 2010 IEEE Int. Conf. on Acoustics, Speech and Signal (ICASSP)*, Texas, USA (2010), p. 2578.
21. A. Bogoni, P. Ghelfi, and F. Laghezza, *Photonics for Radar Networks and Electronic Warfare Systems* (Science Technical, 2019).
22. P. Ghelfi, F. Laghezza, F. Scotti, G. Serafino, A. Capria, S. Pinna, D. Onori, C. Porzi, M. Scaffardi, A. Malacarne, V. Vercesi, E. Lazzeri, F. Berizzi, and A. Bogoni, Nature **507**, 341 (2014).
23. P. Ghelfi, F. Laghezza, F. Scotti, D. Onori, and A. Bogoni, J. Lightwave Technol. **34**, 500 (2016).
24. T. F. Yao, D. Zhu, D. Ben, and S. L. Pan, Opt. Lett. **40**, 1631 (2015).
25. F. Z. Zhang, B. D. Gao, and S. L. Pan, Opt. Express **26**, 17529 (2018).
26. F. Laghezza, F. Scotti, G. Serafino, L. Banchi, V. Malaspina, P. Ghelfi, and A. Bogoni, IET Radar Sonar Navig. **9**, 1040 (2015).
27. A. Malacarne, F. Scotti, S. Maresca, B. Hussain, L. Lembo, G. Serafino, A. Bogoni, and P. Ghelfi, *Proc. of the 45th European Conf. on Optical Communication (ECOC)*, Dublin, Ireland (2019).
28. J. Wang, *Proc. of 2011 IEEE CIE International Conference on Radar*, Chengdu, China (2011), p. 984.
29. Y. Yang and R. S. Blum, IEEE Trans. Signal Process. **59**, 5538 (2011).
30. M. S. Davis and A. D. Lanterman, IEEE Trans. Aerosp. Electron. Syst. **51**, 405 (2015).
31. G. Serafino, P. Ghelfi, P. Pérez-Millán, G. E. Villanueva, J. Palací, J. L. Cruz, and A. Bogoni, J. Lightwave Technol. **29**, 3551 (2011).
32. I. Pasya and T. Kobayashi, *IEEE Phased Array Systems & Technology*, Massachusetts, USA (2013).
33. S. Maresca, G. Serafino, F. Scotti, F. Amato, L. Lembo, A. Bogoni, and P. Ghelfi, *Proc of the 20th International Radar Symposium (IRS)*, Germany (2019).
34. S. Maresca, A. Bogoni, and P. Ghelfi, *Proc. of the 16th European Radar Conference (EuRAD)*, Paris, France (2019).